

Electronic structure and magnetism of the diluted magnetic semiconductor Fe-doped ZnO nano-particles

T. Kataoka¹, M. Kobayashi¹, Y. Sakamoto¹, G. S. Song¹, A. Fujimori^{1,2}, F.-H. Chang³, H.-J. Lin³,
D. J. Huang³, C. T. Chen³, T. Ohkouchi², Y. Takeda², T. Okane², Y. Saitoh², H. Yamagam^{2,4},
A. Tanaka⁵, S. K. Mandal⁶, T. K. Nath⁶, D. Kamarakar^{7,8}, and I. Dasgupta⁹

¹Department of Physics and Department of Complexity Science and Engineering,
University of Tokyo, Bunkyo-ku, Tokyo 113-0033, Japan

²Synchrotron Radiation Research Unit, Japan Atomic Energy Agency, Sayo-gun, Hyogo 679-5148, Japan

³National Synchrotron Radiation Research Center, Hsinchu 30076, Taiwan

⁴Department of Physics, Faculty of Science, Kyoto Sangyo University, Kyoto 603-8555, Japan

⁵Department of Quantum Matter, AD SM, Hiroshima University, Higashi-Hiroshima 739-8530, Japan

⁶Department of Physics & Meteorology, Indian Institute of Technology, Kharagpur 721302, India

⁷Technical Physics & Prototype Engineering Division,

Bhabha Atomic Research Center, Mumbai 400085, India

⁸Present address: Max Planck Institut Fur Festkorperforschung,

Heisenbergstrasse 1, Stuttgart D-70569, Germany

⁹Department of Solid State Physics and Center for Advanced Materials,

Indian Association for the Cultivation of Science, Jadavpur Kolkata 700032, India

(dated: February 21, 2024)

We have studied the electronic structure of $\text{Zn}_{0.9}\text{Fe}_{0.1}\text{O}$ nano-particles, which have been reported to show ferromagnetism at room temperature, by x-ray photoemission spectroscopy (XPS), resonant photoemission spectroscopy (RPES), x-ray absorption spectroscopy (XAS) and x-ray magnetic circular dichroism (XMCD). From the experimental and cluster-model calculation results, we find that Fe atoms are predominantly in the Fe^{3+} ionic state with mixture of a small amount of Fe^{2+} and that Fe^{3+} ions are dominant in the surface region of the nano-particles. It is shown that the room temperature ferromagnetism in the $\text{Zn}_{0.9}\text{Fe}_{0.1}\text{O}$ nano-particles is primarily originated from the antiferromagnetic coupling between unequal amounts of Fe^{3+} ions occupying two sets of nonequivalent positions in the region of the XMCD probing depth of 2-3 nm.

PACS numbers: 74.25.Jb, 71.18.+y, 74.72.Dn, 79.60.-i

I. INTRODUCTION

There is growing interest in diluted magnetic semiconductors (DMs), where magnetic ions are doped into the semiconductor hosts, due to the possibility of utilizing both charge and spin degrees of freedom in the same materials, allowing us to design a new generation spin electronic devices with enhanced functionalities^{1,2}. Theoretical studies on the basis of Zener's p-d exchange model have shown that wide-gap semiconductors such as ZnO doped with transition metal are promising candidates for room temperature ferromagnetic DMs³. First-principle calculations by Sato and Katayama-Yoshida⁴ have also predicted that ZnO-based DMs exhibit ferromagnetism using LSDA calculation. Subsequently a number of experiments on ZnO-based DMs in bulk, thin film and nano-particle forms revealed ferromagnetic properties^{5,6,7,8,9,10}, and among them ZnO-based DMs nano-particles have attracted much attention^{11,12}. Current interest in such magnetic nano-particle systems is motivated by unique phenomena such as superparamagnetism¹³, quantum tunneling of magnetization¹⁴ and particularly magnetism induced by surface defects¹⁵. In the nano-particle form, the structural and electronic properties are modified at the surface as a result of the broken translational symmetry of the

lattice or dangling bond formation, giving rise to weakened exchange coupling, site-specific surface anisotropy, and surface spin disorder^{16,17}. That is, the modification of the electronic structure at the surface of the nano-particles plays a crucial role in the magnetism of this system.

Recently, Kamarakar et al.¹⁸ have reported room temperature ferromagnetism in Fe-doped ZnO nano-particles in the proposed core/shell structure, where Fe^{2+} ions are situated mostly in the core and Fe^{3+} ions in the surface region. However, LSDA+U calculation¹⁹ has indicated the insulating antiferromagnetic state to be more stable than the ferromagnetic state for Fe-doped ZnO system. In view of the presence of Fe^{3+} ions as indicated by local magnetic probes such as electron paramagnetic resonance (EPR) and Mossbauer measurements, Kamarakar et al.¹⁸ have proposed that the presence of surface Zn vacancies that dope hole into the system will be more effective to stabilize the ferromagnetism in this system. However, the correlation between magnetic properties and electronic structure of the Fe-doped ZnO nano-particle semiconductors has not been clarified yet. Thus, investigation of the electronic structure of the Fe-doped ZnO nano-particles is critical to achieve better understanding of this type of nano-materials and to perform new material design. In this paper, we have investigated the electronic structure of $\text{Zn}_{0.9}\text{Fe}_{0.1}\text{O}$ nano-particles using x-ray photo-

photoemission spectroscopy (XPS), vacuum ultraviolet and soft-x-ray resonant photoemission spectroscopy (RPES), x-ray absorption spectroscopy (XAS) and x-ray magnetic circular dichroism (XMCD). RPES is a convenient tool to obtain the Fe 3d partial density of states (PDOS) in the valence-band spectra²⁰. By performing RPES in the Fe 3p-3d core-excitation region, we have studied the electronic states in the surface region with a probing depth of ~ 0.5 nm²¹ of the nano-particles utilizing the surface sensitivity of the technique. On the other hand, RPES in the Fe 2p-3d core-excitation region is more bulk sensitive with a probing depth of ~ 1.5 - 2.0 nm²¹ and enables us to study the electronic structure in both the core and surface regions of the nano-particles. XAS and XMCD, whose probing depth are ~ 2 - 3 nm, enable us to study the element specific electronic structure of the Zn_{0.9}Fe_{0.1}O nano-particles. In particular, XMCD is a powerful tool to study element-specific local magnetic states. Based on our experimental results, we shall discuss the origins of the ferromagnetic properties and magnetic interactions in the Zn_{0.9}Fe_{0.1}O nano-particles.

II. EXPERIMENT

Zn_{0.9}Fe_{0.1}O nano-particles were prepared by the chemical pyrophoric reaction technique. Structural characterization was carried out using x-ray diffraction and transmission electron microscopy (TEM), demonstrating a clear nano-crystal phase. As observed by TEM, the average particle size was around 7 nm with the particle size distribution of 3.0-30.0 nm. Magnetization measurements on the same samples revealed a ferromagnetic-to-paramagnetic transition temperature > 450 K. Details of the sample preparation were described in Ref. [18]. We measured a pressed pellet sample, which after grinding had been calcined at 350. The ferromagnetic moment per Fe as deduced from the SQUID magnetization data was $0.05 \mu_B$ at room temperature¹⁸. XAS and XMCD measurements were performed at the Dargon Beam line BL11A of National Synchrotron Radiation Research Center (NSRRC) in the total-electron-yield (TEY) mode. The monochromator resolution was $\Delta E = E > 10000$ and the circular polarization of x-rays was $\sim 55\%$. XPS measurements using the photon energy of $h\nu = 1253.6$ eV were performed at BL23-SU of SP ring-8. RPES measurements in the Fe 2p-3d and 3p-3d core-excitation regions were performed at BL23-SU of SP ring-8 and at BL-18A of Photon Factory (PF), respectively. For the photoemission measurements, all binding energies (E_B) were referenced to the Fermi level (E_F) of the sample holder which was in electrical contact with the sample. The total energy resolutions of the XPS and RPES measurements were 400 meV and 170 meV, respectively. All the experiments were performed at room temperature.

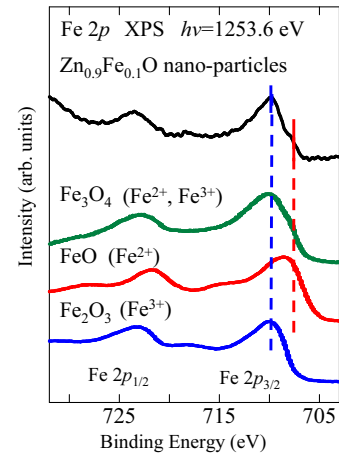


FIG. 1: (Color online) Fe 2p core-level XPS spectrum of the Zn_{0.9}Fe_{0.1}O nano-particles compared with the XPS spectra of Fe₂O₃²², FeO²² and Fe₃O₄²³.

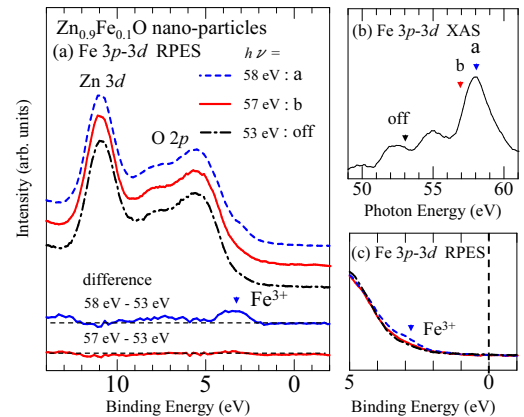


FIG. 2: (Color online) Valence-band photoemission spectra of the Zn_{0.9}Fe_{0.1}O nano-particles. (a) A series of photoemission spectra taken with photon energies in the Fe 3p-3d core-excitation region. Difference curves at the bottom represent the Fe 3d PDOS. (b) Fe 3p-3d XAS spectrum. (c) Magnified view near the valence-band maximum.

III. RESULTS AND DISCUSSION

Figure 1 shows the Fe 2p core-level XPS spectrum of the Zn_{0.9}Fe_{0.1}O nano-particles in comparison with those of Fe₂O₃ (Fe³⁺)²², FeO (Fe²⁺)²² and Fe₃O₄ (Fe³⁺-Fe²⁺ mixed-valence)²³. The Fe 2p_{3/2} peak of the Zn_{0.9}Fe_{0.1}O nano-particles is split into two peaks at $E_B = 710$ eV and 708 eV, corresponding to the energy positions of Fe₂O₃ and FeO. The XPS spectrum of the Zn_{0.9}Fe_{0.1}O nano-particles therefore reflects an Fe³⁺-Fe²⁺ mixed-valent state of the Fe ions in agreement with the previous Mossbauer report¹⁸. In a Fe-doped ZnO system, the valence state of Fe is expected to be +2 if Fe simply substitutes for Zn. The presence of Fe³⁺ ions in this sample has been suggested due to surface Zn

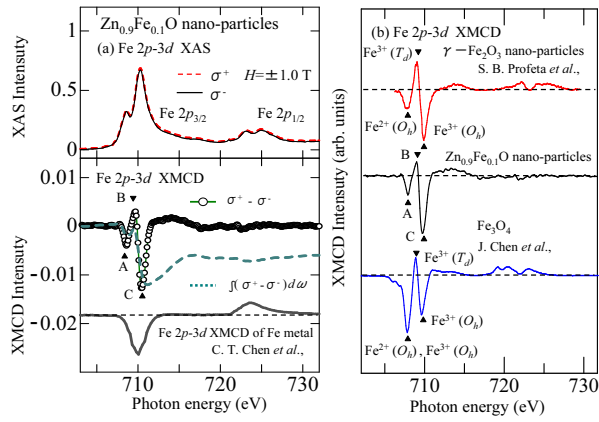


FIG. 3: (Color online) Fe 2p-3d XAS and XMCD spectra of the Zn_{0.9}Fe_{0.1}O nano-particles compared with those of other Fe oxides. (a) Fe 2p-3d XAS spectra in magnetic fields of 1 T. XAS (σ⁺ and σ⁻), XMCD and its integral. The XMCD spectrum of Fe metal is shown for comparison²⁶. (b) XMCD spectrum of the Zn_{0.9}Fe_{0.1}O nanoparticles compared with the XMCD spectra of Fe₂O₃²⁷ and Fe₃O₄²⁸.

vacancies¹⁸ or excess oxygens of the nano-particles.

In order to study the electronic states in the surface region of the nano-particles, we performed RPES measurements in the Fe 3p-3d core-excitation region. RPES in 3d transition metals and their compounds are caused by interference between direct photoemission from the 3d level and Auger-electron emission following the 3p (2p)-3d core-excitation²⁰. Therefore, the difference between valence-band spectra measured on- and off-resonance is used to extract the resonantly enhanced Fe 3d contributions to the valence-band region. Figure 2 (a) shows the valence-band photoemission spectra of the Zn_{0.9}Fe_{0.1}O nano-particles taken with various photon energies in the Fe 3p-3d core-excitation region marked on the Fe 3p-3d XAS spectrum [Fig. 2 (b)]. Figure 2 (c) shows a magnified view near the valence-band maximum. In Fig. 2 (b), one can see that a peak appears at 58 eV, representing the Fe 3p-3d absorption. The same peak is found at 58 eV for Fe₂O₃ (Fe³⁺)²⁴. For FeO (Fe²⁺), on- and off-resonance energies are reported to be 57 and 53 eV, respectively²⁵. From this comparison, we conclude that 3p-3d absorption is mainly due to Fe³⁺ ions. In Fig. 2 (c), one can see that in going from the off-resonance spectrum (hν = 53 eV) to 58 eV, the tail at E_B = 3-4 eV grows in intensity. By subtracting the off-resonance spectrum from the on-resonant ones of Fe³⁺ (hν = 58 eV) and Fe²⁺ (hν = 57 eV), respectively, we have extracted the Fe 3d partial density of states (PDOS) of Fe³⁺ and Fe²⁺ as shown in the bottom panel of Fig. 2 (a). The Fe³⁺ 3d PDOS reveals a feature at E_B = 3-4 eV. On the other hand, the Fe²⁺ 3d PDOS reveals no clear feature. We therefore conclude that the Fe³⁺ ions are dominant in the surface region of the Zn_{0.9}Fe_{0.1}O nano-particles probed by Fe 3p-3d RPES. This, together with the bulk-sensitive Fe 2p-3d RPES result described below, may support the core/shell

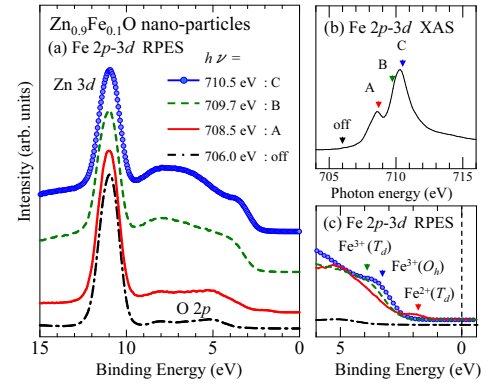


FIG. 4: (Color online) Valence-band photoemission spectra of the Zn_{0.9}Fe_{0.1}O nano-particles. (a) A series of photoemission spectra for photon energies in the Fe 2p-3d core-excitation region. (b) Fe 2p-3d XAS spectrum. (c) Magnified view near the valence-band maximum.

model of the Zn_{0.9}Fe_{0.1}O nano-particles proposed in the previous report¹⁸.

Figure 3 (a) shows the Fe 2p-3d XAS and XMCD spectra of the Zn_{0.9}Fe_{0.1}O nano-particles for opposite magnetization directions recorded using circular polarized x-rays, their difference spectrum, i.e., XMCD spectrum, and its integration. Here, the XAS spectra obtained in the magnetic field of +1.0 T and -1.0 T are denoted by σ⁺ and σ⁻, respectively. The bottom panel shows the XMCD spectrum of Fe metal²⁶. In the XMCD spectrum of the nano-particles, three sharp peaks around hν = 708.5, 709.7 and 710.5 eV, denoted by A, B and C, respectively, are observed. The XMCD spectral line shape of the Zn_{0.9}Fe_{0.1}O nano-particles is different from that of Fe metal, indicating that the magnetism in this sample is not due to segregation of metallic Fe clusters but due to the ionic Fe atoms with localized 3d electrons.

Figure 3 (b) shows the Fe 2p-3d XMCD spectrum of the Zn_{0.9}Fe_{0.1}O nano-particles in comparison with those of Fe₂O₃ nano-particles, where Fe³⁺ ions are both at the tetrahedral (T_d) and octahedral (O_h) sites²⁷, and Fe₃O₄, where Fe³⁺ ions at the T_d and O_h sites and Fe²⁺ ions at the O_h sites coexist²⁸. The XMCD spectrum of the Fe₃O₄, which displays the overlapping contributions from the Fe³⁺ and Fe²⁺ ions, is different from that of the Zn_{0.9}Fe_{0.1}O nano-particles. On the other hand, the spectral line shape of the Fe₂O₃ nano-particles, where XMCD signals are due to Fe³⁺, is similar to that of the Zn_{0.9}Fe_{0.1}O nano-particles. This indicates that the magnetism of the Zn_{0.9}Fe_{0.1}O nano-particles is originated mainly from Fe³⁺ ions and contribution from Fe²⁺ ions appears to be small. By comparison with the Fe 2p-3d XMCD spectral shape of the Fe₂O₃ nano-particles, where XMCD signals are due to Fe³⁺, peaks B and C for the Zn_{0.9}Fe_{0.1}O nano-particles are assigned to Fe³⁺ ions at the T_d and O_h sites, respectively. Although it is likely that peak A arises mainly from Fe³⁺ (O_h) ions, the present Fe 2p-3d RPES result, which is described below, suggests that peak A may be attributed

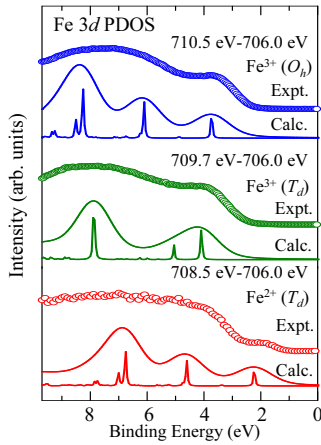


FIG. 5: (Color online) Differences between the on-resonance spectra taken with photon energies marked by A, B and C in Fig. 4 (b) and on-resonance one corresponding to the partial density of states of the Fe ion in each valence state and crystallographic sites. Open circles represent experimental data and thin solid curves indicate calculated spectra.

not only to $\text{Fe}^{3+}(\text{O}_h)$ but also to a small amount of $\text{Fe}^{2+}(\text{T}_d)$ ions.

Figure 4 (a) shows the valence-band photoemission spectra of the $\text{Zn}_{0.9}\text{Fe}_{0.1}\text{O}$ nano-particles taken with various photon energies in the Fe 2p-3d core-excitation region. The Fe 2p-3d XAS spectrum in the same energy region is shown in Fig. 4 (b). The photoemission spectra were taken using photon energies denoted by A, B and C in Fig. 3 and Fig. 4 (b) and at on-resonance ($h\nu = 706.0$ eV). For all the spectra, no photoemission intensity was observed at E_F , indicating the localized nature of the carriers. The on-resonant spectrum of the $\text{Zn}_{0.9}\text{Fe}_{0.1}\text{O}$ nano-particles is similar to that of ZnO showing a sharp peak at about $E_B = 11.0$ eV due to the Zn 3d states as well as a broad feature at $E_B = 4.0-9.0$ eV due to the O 2p band²⁹. If the photon energy is tuned to peak A ($h\nu = 708.5$ eV), one can see a feature at $E_B = 2.0$ eV in the on-resonant spectrum [Fig. 4 (c)], indicating that the intensity of photoelectrons arising from Fe^{2+} ions (the minority-spin state of Fe^{2+} ions³⁰) is enhanced. For the spectra excited by photons with energies corresponding to peaks B ($h\nu = 709.7$ eV) and C ($h\nu = 710.5$ eV), one can see a broad structure around $E_B = 3.0-9.0$ eV [Fig. 4 (a) and (c)]. The spectral line shapes excited by photons corresponding to B and C are similar to each other, indicating that on-resonant spectral line shape strongly depends on the valency of Fe ions rather than coordination as anticipated. To clarify the electronic structure associated with the Fe 3d ion in each valence state and crystallographic site in the $\text{Zn}_{0.9}\text{Fe}_{0.1}\text{O}$ nano-particles, we have performed conduction-band interaction cluster-model calculations to deduce the Fe 3d PDOS of each component^{31,32}.

Figure 5 shows the Fe 3d PDOS (open circles) of

TABLE I: Electronic structure parameters for the $\text{Zn}_{0.9}\text{Fe}_{0.1}\text{O}$ nano-particles used in the cluster-model calculations in units of eV. The charge-transfer energy Δ , the on-site 3d-3d Coulomb energy U_{dd} , and the 3d-2p Coulomb energy U_{dc} on the Fe ion, the hybridization strength between Fe 3d and O 2p $pd\sigma$, and the crystal field $10Dq$.

	Δ	U_{dd}	U_{dc}	$pd\sigma$	$10Dq$
$\text{Fe}^{3+}(\text{O}_h)$	2.0	6.0	7.5	-3.2	0.9
$\text{Fe}^{3+}(\text{T}_d)$	3.5	6.0	7.5	-1.7	-0.7
$\text{Fe}^{2+}(\text{T}_d)$	6.5	5.5	6.9	-1.3	-0.7

the $\text{Zn}_{0.9}\text{Fe}_{0.1}\text{O}$ nano-particles, which has been obtained by subtracting the on-resonance spectrum from the on-resonance ones of $\text{Fe}^{3+}(\text{O}_h)$, $\text{Fe}^{3+}(\text{T}_d)$ and $\text{Fe}^{2+}(\text{T}_d)$, respectively. Calculated spectra (solid curves) are also shown in the same figure. Electronic structure parameters used in the calculations are listed in Table I. For the $\text{Fe}^{3+}(\text{T}_d$ and O_h sites) ions in the Fe-doped ZnO nano-particles, the values of the on-site 3d-3d Coulomb energy U_{dd} and the 3d-2p Coulomb energy U_{dc} on the Fe ion have been taken from the literature on the photoemission study of Fe_3O_4 ²⁸, where Fe^{3+} ions at the T_d and O_h sites and Fe^{2+} ions at the O_h sites coexist. In addition to this, based on the RPES results, we have chosen reasonable values for the charge-transfer energy of the $\text{Fe}^{3+}(\text{T}_d$ and O_h sites) ions. The electronic structure parameters (U_{dd} , U_{dc} and Δ) of the $\text{Fe}^{2+}(\text{T}_d)$ ions were appropriately chosen to reproduce the RPES result since there is no information in the literature about the electronic structure parameters of the $\text{Fe}^{2+}(\text{T}_d)$ ions. The value of the $\text{Fe}^{2+}(\text{T}_d)$ ions thus employed is large compared to those of the $\text{Fe}^{3+}(\text{T}_d)$ ions, consistent with the systematic decrease in the Δ value as the ionic charge increases³³. The calculated spectra have been broadened with a Gaussian having a full width at half maximum (FWHM) of 0.6 eV and with a Lorentzian having a FWHM of 0.2 eV. The spectral line shapes of the calculated results agree with those of experimental results, confirming the presence of the $\text{Fe}^{3+}(\text{O}_h)$, $\text{Fe}^{3+}(\text{T}_d)$ and $\text{Fe}^{2+}(\text{T}_d)$ ions.

Figure 6 (a) and (b) shows the Fe 2p-3d XAS and XMCD spectra of the $\text{Zn}_{0.9}\text{Fe}_{0.1}\text{O}$ nano-particles compared with the calculated spectra of the $\text{Fe}^{3+}(\text{O}_h)$, $\text{Fe}^{3+}(\text{T}_d)$ and $\text{Fe}^{2+}(\text{T}_d)$ ions. The calculations have been made using parameters listed in Table I. One observes shifts of the peaks in the XAS and XMCD spectra for the three kinds of the Fe ions, $\text{Fe}^{3+}(\text{T}_d)$, $\text{Fe}^{3+}(\text{O}_h)$ and $\text{Fe}^{2+}(\text{T}_d)$ ions. The center of gravity of each spectrum is affected by Madelung energy, U_{dd} and U_{dc} at the Fe site, whereas the peak position may be shifted by crystal field splitting²⁸. Therefore, both the coordination and the valence state of the Fe ion affect the XAS and XMCD peak positions. Thus one can clearly distinguish between the

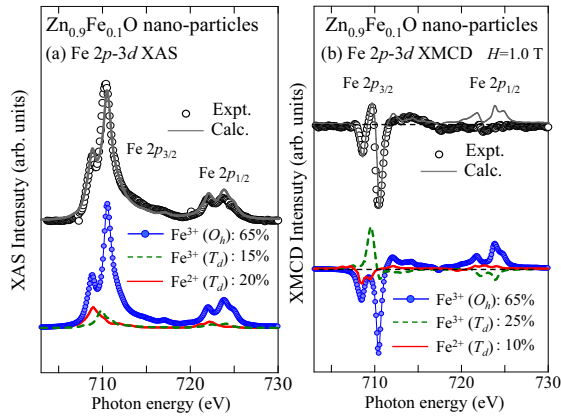


FIG. 6: (Color online) Fe 2p-3d XAS (a) and XMCD (b) spectra of the $\text{Zn}_{0.9}\text{Fe}_{0.1}\text{O}$ nano-particles compared with the calculated one using the cluster-model. Calculated spectra of the $\text{Fe}^{3+}(\text{O}_h)$, $\text{Fe}^{3+}(\text{T}_d)$ and $\text{Fe}^{2+}(\text{T}_d)$ ions at the bottom of each panel have been added to be compared with experiment. Parameters used in the calculations (Table I) were obtained from the analysis of the Fe 2p-3d RPES spectra.

valence and crystal-field of Fe ion [$\text{Fe}^{3+}(\text{T}_d)$, $\text{Fe}^{3+}(\text{O}_h)$ and $\text{Fe}^{2+}(\text{T}_d)$]. In Fig. 6(a), the weighted sum of the calculated $\text{Fe}^{3+}(\text{O}_h)$: 65%), $\text{Fe}^{3+}(\text{T}_d)$: 15%) and $\text{Fe}^{2+}(\text{T}_d)$: 20%) XAS spectra shown at the bottom of panel (a) approximately reproduces the measured XAS spectrum. These ratios indicate that Fe ions are predominantly in the Fe^{3+} state with mixture of a small amount of Fe^{2+} . In Fig. 6(b), the weighted sum of the calculated $\text{Fe}^{3+}(\text{O}_h)$: 65%), $\text{Fe}^{3+}(\text{T}_d)$: 25%) and $\text{Fe}^{2+}(\text{T}_d)$: 10%) XMCD spectra shown at the bottom of panel (b) approximately reproduces the measured XMCD spectrum.

Figure 7(a) shows the Fe 2p-3d XMCD spectra of the $\text{Zn}_{0.9}\text{Fe}_{0.1}\text{O}$ nano-particles measured at various magnetic fields. One can observe the XMCD intensity down to $H = 0.1$ T as shown in Fig. 7(a) and (b), indicating that the ferromagnetism in this sample is originated from the ionic Fe atoms. The difference between the XMCD spectra at $H = 1.0$ and 0.5 T reflects the paramagnetic components as shown in Fig. 7(c). From the line shape of the paramagnetic components analysed with the cluster-model calculation, we conclude that the paramagnetism in the $\text{Zn}_{0.9}\text{Fe}_{0.1}\text{O}$ nano-particles is originated from the Fe^{3+} ions (O_h : 75% and T_d : 25%) and contributions from the Fe^{2+} ions are negligible, consistent with the proposal by Kamakar et al.¹⁸. The ferromagnetic components obtained by subtracting the paramagnetic components from the XMCD spectrum at $H = 0.5$ T is shown in Fig. 7(d). From the line-shape analysis, we conclude that the ferromagnetic components are originated from both predominant Fe^{3+} and a small amount of Fe^{2+} ions, where the composition ratios of the $\text{Fe}^{3+}(\text{O}_h)$, $\text{Fe}^{3+}(\text{T}_d)$ and $\text{Fe}^{2+}(\text{T}_d)$ are about 60%, 25% and 15%, respectively. In Fig. 7(d), peaks due to the Fe^{3+} ions at the T_d and O_h sites occur in the opposite directions.

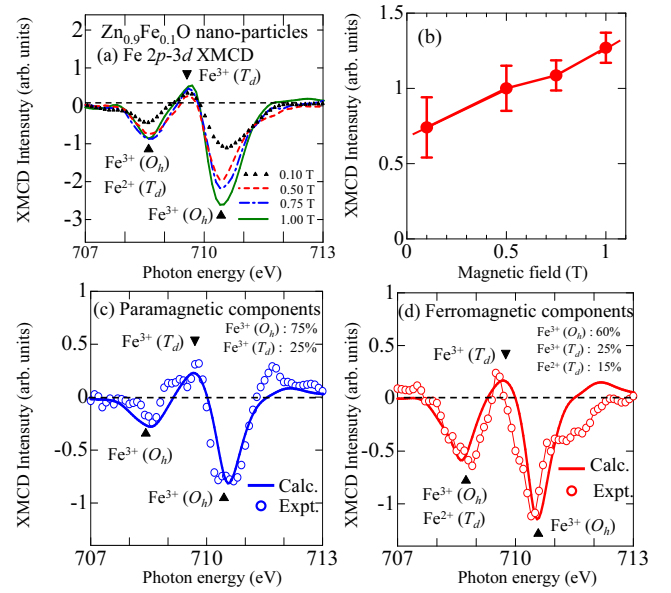


FIG. 7: (Color online) Fe 2p-3d XMCD spectra of the $\text{Zn}_{0.9}\text{Fe}_{0.1}\text{O}$ nano-particles. (a) Fe 2p-3d XMCD spectra of the $\text{Zn}_{0.9}\text{Fe}_{0.1}\text{O}$ nano-particles measured at various magnetic fields. (b) Intensity of Fe 2p-3d XMCD (at $h = 710.5$ eV) as a function of magnetic field. Paramagnetic (c) and ferromagnetic (d) components obtained from the XMCD spectra at 1.0 and 0.5 T. Open circles represent experimental data and thin solid curves indicate calculated spectra.

This clearly implies the presence of $\text{Fe}^{3+}(\text{T}_d)$ - $\text{Fe}^{3+}(\text{O}_h)$ antiferromagnetic coupling. Therefore, it is possible that this sample exhibits "weak ferrimagnetism" due to the Fe^{3+} ions occupying two sets of nonequivalent positions (T_d and O_h sites) in unequal numbers and in antiparallel configurations so that there is a net moment³⁴. That is, the ferromagnetism is caused by the difference in the electron numbers between up and down spins at T_d (O_h) and O_h (T_d) sites. Indeed, the room temperature ferromagnetism of the ferrite Fe_2O_3 due to such Fe^{3+} - Fe^{3+} antiferromagnetic coupling has been reported³⁵. In addition to this, Fe^{2+} - Fe^{2+} , Fe^{3+} - Fe^{3+} exchange interactions and Fe^{3+} - Fe^{2+} double exchange interaction are considered to exist.

From the experimental and cluster-model calculation results, we have estimated the relative abundance of the nonmagnetic/antiferromagnetic (NM/AFM), ferromagnetic (FM) and paramagnetic (PM) components of the Fe ions [$\text{Fe}^{3+}(\text{O}_h)$, $\text{Fe}^{3+}(\text{T}_d)$ and $\text{Fe}^{2+}(\text{T}_d)$] as shown in Fig. 8. The NM/AFM components are originated from the strongly antiferromagnetic coupled Fe ions and are dominant in this sample. On the other hand, the weak ferromagnetic and paramagnetic components are originated mainly from Fe^{3+} as well as from a small amount of Fe^{2+} ions and uncoupled Fe^{3+} ions, respectively. In addition, our analysis confirms the predominance of the $\text{Fe}^{3+}(\text{O}_h)$ and T_d ions in this sample. Considering that the Fe^{3+} ions are dominant in the surface region of the nano-

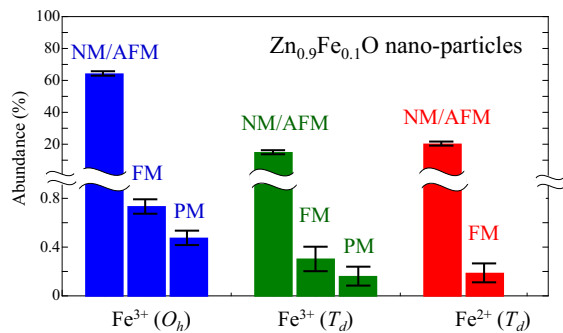


FIG. 8: (Color online) Relative abundance of the nonmagnetic/antiferromagnetic (NM/AFM), ferromagnetic (FM) and paramagnetic (PM) components of the Fe ions [Fe³⁺ (O_h), Fe³⁺ (T_d) and Fe²⁺ (T_d)] in the Zn_{0.9}Fe_{0.1}O nano-particles.

particles probed by surface-sensitive Fe 3p-3d RPES, the presence of the Fe³⁺ must be a surface effect. If Zn vacancies, which dope the system with holes, are present near Fe²⁺ (T_d) ions substituting Zn sites, the Fe²⁺ (T_d) ions will be converted to Fe³⁺ (T_d)¹⁸. This will occur mostly in the surface region of the nano-particles, where the probability of the presence of vacancies is higher. The Fe ions should be at the T_d sites if Fe simply substitutes for Zn site in the Fe-doped ZnO system. One possible origin for the presence of the Fe (O_h) ions is due to the interstitial impurities. However, Karimakar et al. have performed EPR, x-ray diffraction (XRD) and Mossbauer measurements on the same samples and the presence of interstitial impurities has been excluded¹⁸. The other possible origin for the presence of the Fe (O_h) ions is due to excess oxygen at the surface of the nano-particles. According to the literature about the molecular dynamics simulations of Fe₂O₃ nano-particles³⁶, to achieve local charge neutrality, it is expected that oxygen atoms have a tendency to concentrate on the surface of the Zn_{0.9}Fe_{0.1}O nano-particles. Due to the excess oxygen, the Fe ions in the surface region of the Zn_{0.9}Fe_{0.1}O nano-particles are coordinated to a larger number of oxygen atoms as if they were at the O_h sites. Indeed, Chen et al.³⁷ have reported

that Fe (T_d) ions in the surface region of Fe₃O₄ nano-particles have a tendency to be converted to Fe (O_h). In the nano-particle systems, the surface modification may dramatically affect the electronic structure and magnetic properties.

IV. CONCLUSION

In summary, we have performed XPS, RPES, XAS and XMCD measurements on Zn_{0.9}Fe_{0.1}O nano-particles, which exhibit ferromagnetism at room temperature. From the experimental and cluster model calculation results, we find that Fe atoms are predominantly in the Fe³⁺ ionic state with a mixture of a small amount of Fe²⁺ and that Fe³⁺ ions are dominant in the surface region of the nano-particles. It is shown that the room temperature ferromagnetism in the Zn_{0.9}Fe_{0.1}O nano-particles is primarily originated from the antiferromagnetic coupling between unequal amounts of Fe³⁺ ions occupying two sets of nonequivalent positions in the region of the XMCD probing depth of 2-3 nm.

Acknowledgement

We thank T. Koide and D. Asakura for useful discussion and comments. We thank T. Okuda and A. Harasawa for their valuable technical support for the experiment at PF. The experiment at SPRING-8 was performed under the approval of the Japan Synchrotron Radiation Research Institute (JASRI) (proposal no. 2007B3825). The experiment at PF was approved by the Photon Factory Program Advisory Committee (Proposal No. 2006G002). This work was supported by a Grant-in-Aid for Scientific Research in Priority Areas "Creation and Control of Spin Current" (19048012) from MEXT, Japan and a Global COE Program "The Physical Sciences Frontier", from MEXT, Japan and an Indo-Japan Joint Research Project "Novel Magnetic Oxide Nano-Materials Investigated by Spectroscopy and ab-initio Theories" from JSPS, Japan.

¹ J. K. Furdyna, J. Appl. Phys. 64, R29 (1988).

² H. Ohno, Science 281, 951 (1998).

³ T. Dietl, H. Ohno, F. Matsukura, J. Cibert and D. Ferrand, Science 287, 1019 (2000).

⁴ K. Sato and H. Katayama-Yoshida, Jpn. J. Appl. Phys. 40, L334 (2001).

⁵ A. C. Tuan, J. D. Bryan, A. B. Pakhomov, V. Shutthanandan, S. Thevuthasan, D. E. McCreedy, D. Gaspar, M. H. Engelhard, J. W. Rogers, Jr., K. Krishnan, D. R. Gamelin and S. A. Chambers, Phys. Rev. B 70, 054424 (2004).

⁶ K. Ueda, H. Tabata and T. Kawai, Appl. Phys. Lett. 79, 988 (2001).

⁷ P. Sharma, A. Gupta, K. V. Rao, F. J. Owens, R. Sharma, R. Ahuja, J. M.orio, G. B. Johansson and G. A. Gehring, Nat. Mater. 2, 673 (2003).

⁸ D. A. Schwartz and D. R. Gamelin, Adv. Mater. 16, 2115 (2004).

⁹ P. V. Radovanovic and D. R. Gamelin, Phys. Rev. Lett. 91, 157202 (2003).

¹⁰ T. Meln and G. Markovich, J. Phys. Chem. B 109, 20232 (2005).

¹¹ S. K. Mandal, A. Das, T. N. Nath, D. Karimakar and B. Satpati, J. Appl. Phys. 100, 104315, (2006).

¹² S. K. Mandal, T. N. Nath, A. Das and R. K. Karimakar, Appl.

- Phys. Lett. 89, 162502 (2006).
- ¹³ C. Kittel, Phys. Rev. 70, 965 (1946).
 - ¹⁴ E. M. Chudnovsky and L. Gunther, Phys. Rev. Lett. 60, 661 (1988).
 - ¹⁵ M. A. Garcia, J. M. Merino and E. Fernandez, Nano Lett. 7, 1489 (2007).
 - ¹⁶ C. Q. Sun, Progress in Solid State Chem. 35, 1 (2007).
 - ¹⁷ R. H. Kodama, A. E. Berkowitz, Jr E. J. McNiff and S. Foner, Phys. Rev. Lett. 77, 394 (1996).
 - ¹⁸ D. Kamarakar, S. K. Mandal, R. M. Kadam, P. L. Paulose, A. K. Rajarajan, T. K. Nath, A. K. Das, I. Dasgupta, and G. P. Das, Phys. Rev. B. 75, 144404 (2007).
 - ¹⁹ P. Gopal and N. A. Spaldin, Phys. Rev. B 74, 094418 (2006).
 - ²⁰ L. C. Davis, J. Appl. Phys. 59, R25 (1986).
 - ²¹ I. Lindau and W. E. Spicer, J. Electron Spec. Rel. Phen. 3, 409 (1974).
 - ²² P. Graat and M. A. J. Somers, Surf. Interface Anal. 26, 773 (1998).
 - ²³ T. Fujii, F. M. F. de Groot, and G. A. Sawatzky, F. C. Voogt, T. H. Ibm a and K. Okada, Phys. Rev. B 59, 3195 (1999).
 - ²⁴ R. J. Lad and V. E. Henrich, Phys. Rev. B 39, 13478 (1989).
 - ²⁵ A. Fujimori, M. Saeki, N. Kinoshita, M. Taniguchi and S. Suga, Phys. Rev. B 34, 7318 (1986).
 - ²⁶ C. T. Chen, Y. U. Idzerda, H.-J. Lin, N. V. Smith, G. Meigs, E. Chaban, G. H. Ho, E. Pellegrin and F. Sette, Phys. Rev. Lett. 75, 152 (1995).
 - ²⁷ S. B. Profeta, M. A. Arias, E. Tronc, I. Letard, C. C. D. Moulins and P. Saintavrit, Phys. Scripta. T 115, 626 (2005).
 - ²⁸ J. Chen, D. J. Huang, A. Tanaka, C. F. Chang, S. C. Chung, W. B. Wu and C. T. Chen, Phys. Rev. B 69, 085107 (2004).
 - ²⁹ M. G. Abas, S. G. Ota, J. R. R. Barrado, M. Sanchez and N. T. Barrett, Appl. Phys. Lett. 86, 042104 (2005).
 - ³⁰ J. Takaobushi, M. Ishikawa, S. Ueda, E. Ikenaga, J.-J. Kim, M. Kobata, Y. Takeda, Y. Saitoh, M. Yabashi, Y. Nishino, D. Miwa, K. Tamasaku, T. Ishikawa, I. Satoh, H. Tanaka, K. Kobayashi and T. Kawai, Phys. Rev. B 76, 205108 (2007).
 - ³¹ A. Tanaka and T. Jo, J. Phys. Soc. Jpn. 63, 2788 (1994).
 - ³² A. Tanaka and T. Jo, J. Phys. Soc. Jpn. 61, 2669 (1992).
 - ³³ A. E. Bocquet, T. Mizokawa, T. Saitoh, H. Namatame and A. Fujimori, Phys. Rev. B 46, 3771 (1992).
 - ³⁴ M. A. Gillo, Phys. Rev. 109, 777 (1958).
 - ³⁵ X. Boa, G. Lia, X. Q. Liu, Y. Xue and L. Li, J. Solid State Chem. 180, 1038 (2007).
 - ³⁶ B. T. H. L. Khanh, V. V. Hoang and H. Zung, Eur. Phys. J. D. 49, 325 (2008).
 - ³⁷ L. X. Chen, T. Liu, M. C. Thumauer, R. C. Sencsits and T. Raj, J. Phys. Chem B 106, 8539 (2002).